Self-consistent local equilibrium model for density profile and distribution of dissipative currents in a Hall bar under strong magnetic fields

Kaan Güven and Rolf R. Gerhardts
Max-Planck-Institut für Festkörperforschung, Heisenbergstrasse 1, D-70569 Stuttgart, Germany
(Received 8 October 2002; published 24 March 2003)

Recent spatially resolved measurements of the electrostatic-potential variation across a Hall bar in strong magnetic fields, which revealed a clear correlation between current-carrying strips and incompressible strips expected near the edges of the Hall bar, cannot be understood on the basis of existing equilibrium theories. To explain these experiments, we generalize the Thomas-Fermi-Poisson approach for the self-consistent calculation of electrostatic potential and electron density in *total* thermal equilibrium to a *local equilibrium* theory that allows us to treat finite gradients of the electrochemical potential as driving forces of currents in the presence of dissipation. A conventional conductivity model with small values of the longitudinal conductivity for integer values of the (local) Landau-level filling factor shows that, in apparent agreement with experiment, the current density is localized near incompressible strips, whose location and width in turn depend on the applied current.

DOI: 10.1103/PhysRevB.67.115327 PACS number(s): 73.40.−c,73.50.Jt

I. INTRODUCTION

The question, where the current flows in a Hall bar under quantum-Hall-effect (QHE) conditions, has been investigated by many authors, and many controversial answers have been given. Part of this controversy arises from the fact that, apart from the total electric current density, different partial current densities can be defined which integrate to the same total current.[1] Even in the thermodynamic equilibrium state with vanishing total current, quantum calculations yield finite current densities which are related to the density variation and the energy dispersion of the two-dimensional electron gas (2DEG) near the sample edges. Such current distributions have been calculated using different approaches, from simple Hartree-type approximations[2] to sophisticated treatments of exchange and correlation effects within a current-density functional theory.[3,4] Unfortunately, there is little experimental information about the current-density distribution in samples with zero or small total current. Experiments with high currents, of the order of the critical current for the breakdown of the QHE, have shown that the current distribution depends strongly on the mobility of the sample,[5] but also on screening effects caused by nearby metallic gates[6] or mesoscopic inhomogeneities like arrays of antidots.[7,8]

Our present work is motivated by a recent series of experiments,[9–11] in which a scanning force microscope[12] is used to measure the Hall-potential distribution across a Hall bar under QHE conditions. The characteristics of the potential distribution are found to change drastically with the magnetic field applied perpendicularly to the sample, i.e., with the Landau-level filling factor ν. Typical experimental results for $\nu\sim 2$ are reproduced in Fig. 1, and similar results have been obtained around $\nu=4$.[10] While for ν values far away from integers the potential varies linearly across the sample (''type I'' behavior, seen in Fig. 1 for $\nu=1.67$, 1.76, and 2.73) and for integer and slightly lower values a nonlinear potential drop in a broad region in the middle of the sample is observed (''type II,'' seen for $1.96\lesssim\nu\lesssim 2.09$), for slightly larger than integer ν values the potential is flat in the center region and drops across two strips that move with increasing ν towards the sample edges (''type III,'' seen at $2.14\leqslant\nu\leqslant 2.50$). The position and width of these strips coincide with those of the incompressible strips[10] that are expected to form in the sample due to the nonlinear screening properties of the 2DEG in strong magnetic fields.[13–15]

The fact that the Hall voltage drops across the incompressible strips indicates that the current flows preferably along these strips. Such a conjecture can be found in an early paper by Chang.[16] Self-consistent equilibrium calculations, which imposed a dissipationless Hall current as a thermodynamic boundary condition on the 2DEG in a Hall bar,[17,18] could, however, not confirm this conjecture. On the contrary, the current-density profile was found to extend over the whole sample width and to follow closely the electron-density profile. On the other hand, there is a simple classical

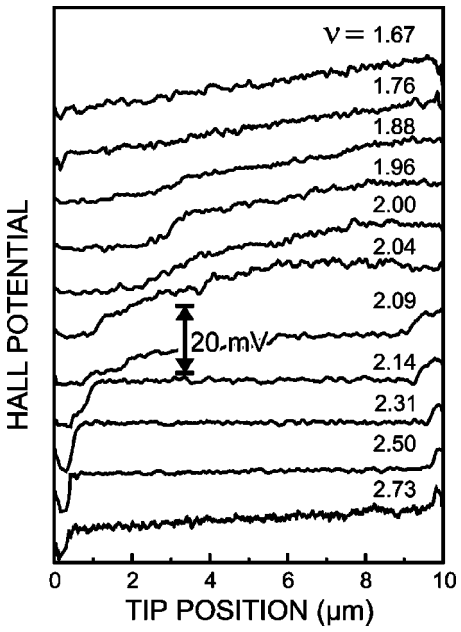

FIG. 1. Measured Hall-potential profile for different magnetic fields around filling factor $\nu=2$, after Ref. 10.

argument supporting Chang's conjecture. If we describe the magnetotransport in the inhomogeneous Hall bar by a local Ohm's law with a position-dependent resistivity tensor $\hat{\rho}$, we find that the current density is largest where the longitudinal resistivity is smallest, i.e., along the incompressible strips, if we assume that $\hat{\rho}(\nu)$ depends on the local filling factor in the same manner as for a homogeneous sample. Such a classical local magnetotransport model has previously been used to explain, for inhomogeneous samples, a finite width of quantum Hall plateaus without the assumption of localized states and to simulate the magnetic-field dependence of Hall-type voltages in Hall bars with internal contacts.[19,20] More recently such a local model has also proved useful for the understanding of the current and electric-field distribution in antidot systems close to the breakdown of the QHE.[8,21]

Since the dissipative nonequilibrium current will lead to a position-dependent electrochemical potential, which changes the equilibrium electron-density and electrostatic-potential distribution, we have to generalize the Thomas-Fermi-Poisson scheme for the self-consistent calculation of the latter to include the current-induced changes. This will be done in Sec. II. Typical results obtained from this approach are presented in Sec. III. In Sec. IV we will discuss the most relevant results in the light of the motivating experiments,[10] and we will comment on apparent limitations of our model. Some preliminary results of this work have been presented previously.[22]

II. MODEL

Following previous work[14,18] we model the Hall bar as a 2DEG in the plane $z=0$, being restricted to the strip $|x|<d$ and translation invariant in the y direction. Physically, the confinement potential of the 2DEG is produced by a homogeneous background charge in the strip, so that the density of free charges has the form $\rho(x)\delta(z)$ with

$$\rho(x)=e[n_0-n_{\rm el}(x)]\theta(d^2-x^2), \tag{1}$$

with $n_{\rm el}(x)$ and n_0 the surface densities of 2DEG and background, respectively. Electrostatic boundary conditions are fixed by the assumption of metallic half-planes of constant potentials V_L and V_R in $z=0$, $x<-d$, and in $z=0$, $x>d$, respectively, and by dielectric constants $\kappa_>$ and $\kappa_<$ in the half-spaces $z>0$ and $z<0$. With these assumptions, for $z\neq 0$ the electrostatic potential $V(x,z)=\mathrm{Im}\,F(\zeta)$ satisfies the Laplace equation and can be written as the imaginary part of an analytic function $F(\zeta)$ of the complex variable $\zeta=x+iz$, which is determined by its boundary conditions on the real axis.[23,13,14]

We shall recall briefly the use of this electrostatic model for the description of the thermodynamic equilibrium state[15,18] and then propose an extension to current-carrying stationary nonequilibrium states.

A. Thermal equilibrium

To determine $n_{\rm el}(x)$ we need the electrostatic potential $V(x)=V(x,z=0)$ in $|x|\leq d$. It can be written as the sum of three terms,

$$V(x)=V_0(x)+V_{\rm g}(x)+V_H(x), \tag{2}$$

where

$$V_{\rm g}(x)=\frac{V_L+V_R}{2}+\frac{V_R-V_L}{\pi}\arcsin\left(\frac{x}{d}\right) \tag{3}$$

is determined by the potential values on the in-plane gates and accompanied by compensating induced charges on the gates. The free charges determine $V(x,z)=\mathrm{Im}\,F(\zeta)$ with[18] (we write the potential as potential energy of an electron, i.e., including a factor $-e$)

$$\frac{dF}{d\zeta}=\frac{i}{\pi w(\zeta)}\int_{-d}^{d}dx\frac{\sqrt{d^2-x^2}}{\zeta-x}\frac{2\pi e}{\bar{\kappa}}\rho(x), \tag{4}$$

where $w(\zeta)=\sqrt{d^2-\zeta^2}$ is analytic except on cuts at $z=0$, $|x|\geq d$, and $\bar{\kappa}=(\kappa_>+\kappa_<)/2$. By integration one obtains the (bare) confinement potential for $n_{\rm el}(x)\equiv 0$ as

$$V_0(x)=-E_0\sqrt{1-\left(\frac{x}{d}\right)^2},\quad E_0=\frac{2\pi e^2}{\bar{\kappa}}n_0 d. \tag{5}$$

The Hartree potential due to the 2DEG follows as

$$V_H(x)=\frac{E_0}{\pi n_0}\int_{-1}^{1}d\xi' K\left(\frac{x}{d},\xi'\right)n_{\rm el}(\xi' d), \tag{6}$$

with the kernel[18]

$$K(\xi,\eta)=\ln\left|\frac{\sqrt{(1-\xi^2)(1-\eta^2)}+1-\xi\eta}{\xi-\eta}\right|. \tag{7}$$

The electron density is, in turn, determined by the potential $V(x)$. We assume that $V(x)$ varies slowly on the scale of typical quantum mechanical lengths, notably the magnetic length $l_m=\sqrt{\hbar/m\omega_c}$ defined by the cyclotron frequency $\omega_c=eB/mc$, and calculate the electron density in the Thomas-Fermi approximation

$$n_{\rm el}(x)=\int dE D(E) f(E+V(x)-\mu^*), \tag{8}$$

where $f(E)=1/[1+\exp(E/k_BT)]$ is the Fermi distribution and $D(E)$ the (single particle) density of states (DOS) of the 2DEG. For the Hall bar in the absence of a magnetic field, $B=0$, we take $D(E)=D_0\theta(E)$, with $D_0=m/(\pi\hbar^2)$, while for large B we will use a (suitably broadened) Landau DOS.

Solving Eqs. (2) and (8) self-consistently for *constant* electrochemical potential μ^*, we obtain the electron density and the electrostatic potential in the thermal equilibrium state. The value of μ^* determines the average electron density and vice versa (for fixed T, B, etc.).

B. Local equilibrium with imposed current

If a stationary net current is imposed on the Hall bar, this leads to position-dependent current densities and electric fields which, in the linear response regime, are interrelated by Ohm's law. The relevant field driving the net current is the gradient of the electrochemical potential, $\nabla\mu^*$, which

vanishes in thermal equilibrium. In view of Eq. (8), we should expect that a position-dependent μ^* will lead to a modified electron density $n_{\rm el}(x)$ and this, according to Poisson's equation, to a modified electrostatic potential. Our aim is to extend the self-consistent Thomas-Fermi-Poisson approximation for the thermal equilibrium state to the stationary nonequilibrium situation defined by the imposed current. To do so, we adopt the widely used assumption of *local equilibrium*: thermodynamic variables are assumed to vary only slowly in space and to satisfy locally the same relations as they would do in a homogeneous thermodynamic equilibrium state. Then, for a given position-dependent $\mu^*(x)$, we can use again Eqs. (2) and (8) to calculate $V(x)$ and $n_{\rm el}(x)$.

We will now formulate a model that allows us to calculate $\nabla\mu^*$, and thus the position-dependent electrochemical potential up to a constant, provided the electron density $n_{\rm el}(x)$ and the total current

$$I=\int_{-d}^{d} dx j_y(x,y) \tag{9}$$

are given. In the spirit of the Thomas-Fermi and the local equilibrium approximation, which assume that electrostatic potentials and thermodynamic variables vary on a scale much larger than quantum lengths, we also assume that the current density $\mathbf{j}(\mathbf{r})=(j_x(x,y),j_y(x,y))$ and the electric field satisfy the local version of Ohm's law,

$$\hat{\rho}(\mathbf{r})\mathbf{j}(\mathbf{r})=\mathbf{E}(\mathbf{r})\equiv\nabla\mu^*(\mathbf{r})/e, \tag{10}$$

where the resistance tensor $\hat{\rho}(\mathbf{r})=[\hat{\sigma}(n_{\rm el}(\mathbf{r}))]^{-1}$ is assumed to depend on position only via the electron density $n_{\rm el}(\mathbf{r})$.

Assuming a stationary situation with translation invariance in y direction (i.e., $\hat{\rho}$, $\mathbf{j}$, and $\mathbf{E}$ are independent of y), we obtain from the Maxwell equations $\nabla\cdot\mathbf{j}(\mathbf{r})=0$ and $\nabla\times\mathbf{E}(\mathbf{r})=\mathbf{0}$ that the current density j_x across and the field E_y along the bar are independent of x,

$$j_x\equiv 0, \quad E_y(x)\equiv E_y^0. \tag{11}$$

With $\rho_{yy}=\rho_{xx}=\rho_l(x)$ the longitudinal and $\rho_{xy}=-\rho_{yx}=\rho_H(x)$ the Hall resistivity, we further get

$$j_y(x)=\frac{1}{\rho_l(x)}E_y^0, \quad E_x(x)=\frac{\rho_H(x)}{\rho_l(x)}E_y^0. \tag{12}$$

From these results we obtain

$$\mu^*(x,y)=\mu_0^*+eE_y^0\left\{y+\int_0^x dx'\frac{\rho_H(x')}{\rho_l(x')}\right\}, \tag{13}$$

where μ_0^* occurs as an undefined constant, and from Eq. (9) we get the normalization

$$E_y^0=\frac{I}{\displaystyle\int_{-d}^{d} dx[1/\rho_l(x)]}. \tag{14}$$

The new self-consistency problem for the stationary state is completely defined, if we choose a model for the dependence of the conductivity tensor on the electron density. To solve it iteratively, we start with zero current $I=0$ and solve the old equilibrium problem. Then we take a fixed value $I\neq 0$ and proceed as follows.

In the next step of the new iteration, we use $n_{\rm el}(x)$ from the previous step and calculate for the given I the electrochemical potential (13). Then we put this into Eq. (8). To compensate the y-linear term, we add an identical term to the electrostatic potential. This guarantees that the electron density remains independent of y. Then we solve the ''old'' problem, Eqs. (2) and (8) with the modified x-dependent electrochemical potential, self-consistently to determine $V(x)$ and $n_{\rm el}(x)$, choosing μ_0^* so that the average electron density remains the same as without current. Convergence of the ''old'' problem completes this step of the new iteration. The steps of the new iteration are repeated until there is practically no further change of $n_{\rm el}(x)$.

We have performed these self-consistent calculations for two types of electrostatic boundary conditions. First we started with a symmetric electron profile and $V_G=V_R-V_L=0$, and assumed that an applied current does not change the potentials of the in-plane gates. Then, in a strong magnetic field and under an imposed current, we obtain an asymmetric electron profile that is shifted towards one of the sample edges. This is an obvious consequence of the Lorentz force on the drifting electrons. In this situation, the applied current leads to a change of the induced charges in the in-plane gates.

Since $\partial V(x,z)/\partial z=\mathrm{Re}[dF/d\zeta]$, we can use Eq. (4) to calculate the induced charge density in the in-plane gates, $\rho_{\rm ind}(x)=[\overline{\kappa}/(2\pi e)]\mathrm{Re}\,F'(x+i0^+)$. For the total induced charge $Q_R=\int_d^\infty dx\rho_{\rm ind}(x)$ in the right gate this yields

$$\frac{Q_R}{en_0d}=-\frac{2}{\pi}\int_{-1}^{1} d\xi\left[1-\frac{n_{\rm el}(\xi d)}{n_0}\right]\arctan\sqrt{\frac{1+\xi}{1-\xi}}. \tag{15}$$

The corresponding result Q_L for the left gate is obtained from Eq. (15) by replacing ξ under the square root by $-\xi$. The sum of these induced charges compensates the free charges, $Q_R+Q_L=-\int_{-d}^{d}dx\rho(x)$, and their difference vanishes if the electron density is symmetric, $n_{\rm el}(-x)=n_{\rm el}(x)$.

The asymmetric density profile, resulting for the current-carrying stationary state from the requirement $V_G=0$, leads to $Q_R\neq Q_L$. Since Q_R+Q_L is kept constant, this means that charge must flow from one gate to the other as the stationary state is established. As an alternative electrostatic boundary condition, which may be more realistic in certain situations, we investigated the ''floating gate'' condition, requiring that Q_R (and thus Q_L) be kept constant and a finite voltage between the in-plane gates build up.

III. RESULTS

A. Classical regime

In the classical regime of low magnetic field and high temperature, the magnetic field should not affect the thermodynamic equilibrium state[24] (Bohr–van-Leeuwen theorem).

Therefore, we use the simple DOS $D(E)=D_0\theta(E)$, which for zero temperature renders Eq. (6) as

$$V_H(\xi d)=\frac{1}{\alpha}\int_{\beta_L}^{\beta_R} d\xi' K(\xi,\xi')[E_F-V(\xi' d)], \qquad (16)$$

where the dimensionless parameters $\beta_L<\beta_R$ define the edges of the density profile, $V(\beta_L d)=V(\beta_R d)=E_F=\mu^*(T=0)$, and where

$$\alpha=\pi n_0/(E_0 D_0)=\pi a_0/d, \qquad (17)$$

with $a_0=\bar{\kappa}\hbar^2/(2me^2)$ the screening length. [Due to a misprint, in the denominator in Eq. (15) of Ref. 18 the factor π is missing.] Together with Eq. (2), Eq. (16) represents a linear integral equation for $V(\xi d)$ in the interval $\beta_L\leqslant\xi\leqslant\beta_R$, which can easily be solved numerically. Solutions of this linear equation are used as starting points for all numerical calculations at finite temperature and magnetic field, which lead to nonlinear integral equations that must be solved iteratively.

As has been shown in Ref. 18, with decreasing values of α screening becomes more effective, and a voltage V_G applied across the bar leads to a shift and deformation of the equilibrium electron density profile $n_{\rm el}(x)$. At finite temperature, the sharp edges of the zero-temperature profiles are smeared out.

In the nonequilibrium calculations, we use the Drude model for the resistivity tensor,

$$\rho_l(x)=1/\sigma_0(x), \quad \rho_H(x)=\omega_c\tau\rho_l(x), \qquad (18)$$

with $\sigma_0(x)=(e^2\tau/m)n_{\rm el}(x)$. Then, according to Eq. (12), the current density $j_y(x)=\sigma_0(x)E_y^0$ is proportional to the electron density, and $E_x(x)=\omega_c\tau E_y^0$ is constant. Strictly speaking the last result, which follows from the fundamental linear response equation $j_x(x)=\sigma_{xx}(x)[E_x-\omega_c\tau E_y]\equiv 0$, can be justified from our local approach only at positions x where $n_{\rm el}(x)\neq 0$. On the other hand, within our local equilibrium model we expect the electrochemical potential to be constant in regions where no (dissipative) current flows and where no electrons are. Therefore we put $E_x(x)=0$ if $n_{\rm el}(x)=0$. In practical calculations we use

$$E_x(x)=\omega_c\tau E_y^0\theta(n_{\rm el}(x)/n_0-\epsilon), \qquad (19)$$

with $\epsilon=10^{-4}$, which defines effective edges $b_L<b_R$ of the density profile by $n_{\rm el}(b_L)=n_{\rm el}(b_R)=\epsilon n_0$.

Typical results are shown in Fig. 2, where for the current-carrying states the variation of the electrochemical potential, $\Delta\mu^*\equiv\mu^*(b_R)-\mu^*(b_L)=(b_R-b_L)\omega_c\tau E_y^0$, is fixed as $u_H=\Delta\mu^*/E_0=0.2$. This yields the current $I=u_H[2d/(b_R-b_L)](e^2\bar{n}_{\rm el}/m\omega_c)E_0/e$, where $2d\bar{n}_{\rm el}=\int_{-d}^{d}dx\, n_{\rm el}(x)$ is fixed, $\bar{n}_{\rm el}/n_0=0.6278$. We observed that, for fixed vanishing gate voltage and $0<u_H\lesssim 0.2$, the shift (and deformation) of the density profile increases roughly linearly with u_H. Under floating gate conditions, for $u_H=0.2$ a voltage $V_R-V_L=0.319E_0$ builds up between the in-plane gates. This is larger than the linear extrapolation $u_H[2d/(b_R-b_L)]E_0$ due to the singular slopes of the self-consistent potential at the edges of the gates (see Fig. 2). Figure 2 shows that, over the whole range of finite density, the self-consistently calculated total potential $V(x)$ follows very closely the linear position dependence of the electrochemical potential. This observation holds for both fixed-gate-voltage and floating-gate-boundary conditions. In the following we will consider only the more realistic floating-gate-boundary conditions.

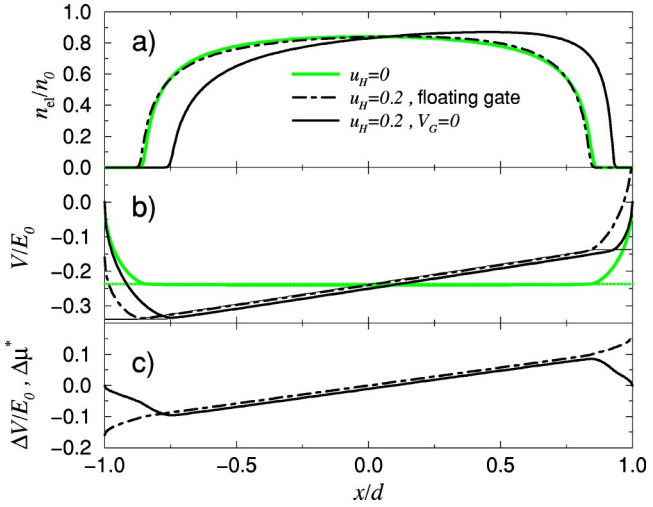

FIG. 2. (a) Density profile $n_{\rm el}(x)$ and (b) total potential $V(x)$ in equilibrium (gray lines) and with current $I\propto u_H$ (black lines) for fixed gate voltage $V_R=-V_L=0$ (solid line) and for floating gates (dash-dotted lines), and (c) induced Hartree potentials $V(x;I)-V(x,0)$ for both cases. The thin lines indicate the electrochemical potentials $\mu^*(x)$. $\alpha=0.01$, $\beta_R=-\beta_L=0.848$.

B. Quantum regime

For strong, quantizing magnetic fields we should use a suitable form of a broadened Landau DOS

$$D(E)=\frac{g_s}{2\pi l_m^2}\sum_{n=0}^{\infty}A_n(E), \qquad (20)$$

where $A_n(E)$ is the spectral function of the nth Landau level with energy eigenvalue $\varepsilon_n=\hbar\omega_c(n+1/2)$, and $g_s=2$ accounts for spin degeneracy. The model to be used for the resistivity tensor should show the characteristic behavior known from the quantum Hall regime, notably (nearly) vanishing $\rho_l(x)$ at (even) integer local filling factor $\nu(x)=2\pi l_m n_{\rm el}(x)$. Moreover, the approximations for the conductivity tensor and the DOS should satisfy certain consistency relations (consequences of the equation of continuity).[27] However, before we address such sophisticated questions we want to present a very simple model.

1. Simplified model

First we follow previous work[15,18] and consider the bare Landau DOS, taking in Eq. (20) $A_n(E)=\delta(\varepsilon_n-E)$. This leads, in thermal equilibrium, to the appearance of incompressible strips of finite width at integer values of the local filling factor. The temperature dependence of these strips has been discussed in Ref. 15, and the dependence of position

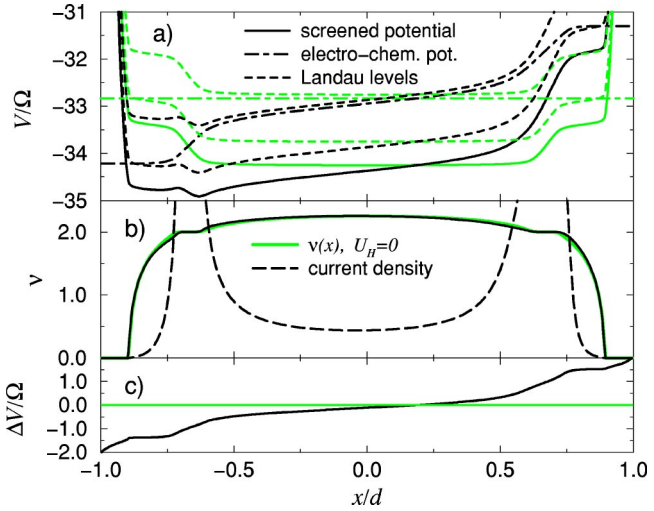

FIG. 3. (a) Self-consistent potential $V(x)$ and (b) normalized density $\nu(x)$ for zero (thick solid gray) and finite (thick solid black lines) current, calculated for model (22) with $\epsilon=0.002$. a) also shows the corresponding $\mu^*(x)$ (dash-dotted lines) and the Landau levels $V(x)+\Omega(n+1/2)$ (dashed lines), and (b) the current density (long-dashed line, arbitrary units). (c) shows the current-induced change of the self-consistent potential (black). Model parameters (see text) are $\alpha=0.02$, $\Omega\equiv\hbar\omega_c=E_0/200$, $k_BT/\Omega=0.04$, $U_H\equiv\Delta\mu^*=3\Omega$.

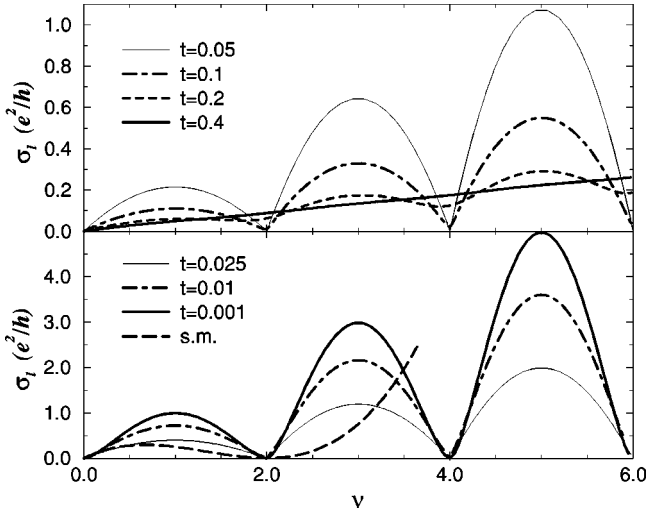

FIG. 4. Longitudinal conductivity σ_l vs filling factor ν for the Gaussian model (23) with $\Gamma/\hbar\omega_c=0.035$ for (a) high and (b) low values of the reduced temperature $t=k_BT/\hbar\omega_c$. The thick solid curves coincide with the limits for high temperature [$k_BT>\hbar\omega_c$, (a)] and zero temperature [$k_BT\ll\Gamma$, (b)]. The long-dashed curve in (b) indicates the model (22).

and width of the strips on magnetic field and applied gate voltage V_R-V_L has been investigated in Refs. 18 and 25 for the present Hall bar geometry. To investigate the effect of an imposed current, we first use a simplistic model for the resistance tensor, which has been used successfully for the calculation of the current density in an antidot system in a strong magnetic field.[21,26] For $\sigma_{yx}(x)=-\sigma_{xy}(x)=\sigma_H(x)$ we take

$$\sigma_H(x)=(e^2/h)\,\nu(x), \tag{21}$$

which yields the correct values at integer filling factors, but no quantum Hall plateaus. To simulate the behavior of $\sigma_{xx}=\sigma_{yy}=\sigma_l$ near integer filling $\nu=2$, we approximate[21] the longitudinal conductivity as

$$\sigma_l(x)=\sigma_H(x)\{\epsilon+[2-\nu(x)]^2/4\}, \tag{22}$$

with a small but finite positive value ϵ ($\sim10^{-3}$) to avoid divergencies. This describes correctly that $\rho_l(x)\propto\sigma_l(x)$ becomes very small at the incompressible strips with local filling factor $\nu(x)=2$, although the analytical dependences for $\nu\neq2$ are not correct [see Fig. 4(b) below].

Nevertheless, this simple model is able to reproduce characteristic features observed in the experiment[10] as is shown in Fig. 3. The current flows preferably along the incompressible strips, where $\nu(x)=2$ and the longitudinal resistivity is smallest, and there the gradient of $\mu^*(x)$ is largest. Due to the Thomas-Fermi-Poisson self-consistency requirement, the total potential $V(x)$ is forced to follow $\mu^*(x)$ closely, so that the current-induced change of the electron density profile is small (which keeps the change of electrostatic energy small). The induced $\Delta V(x)$ follows closely $\mu^*(x)$ and varies mainly in the region of incompressible strips.

2. Gaussian-level broadening

As a more realistic model for the longitudinal conductivity we use the Gaussian model[27]

$$\sigma_l=\frac{e^2g_s}{h}\int_{-\infty}^{\infty}dE\left[-\frac{df}{dE}\right]\sum_{n=0}^{\infty}\left(n+\frac{1}{2}\right)[\sqrt{\pi}\Gamma A_n(E)]^2, \tag{23}$$

with the spectral function

$$A_n(E)=\frac{\exp(-[\varepsilon_n-E]^2/\Gamma^2)}{\sqrt{\pi}\Gamma}, \tag{24}$$

which then, for consistency reasons, should also be used in the DOS, Eq. (20). An alternative, which leads to qualitatively the same results, would be to use the self-consistent Born approximation[20,28] which would replace the normalized Gaussians by normalized half-ellipses. To avoid divergencies, we replace σ_l of Eq. (23) for $\nu>1$ by $\max(\sigma_l,\sigma_H/10^4)$.

Together with $\nu=2\pi l_m^2\int dE f(E-\mu)D(E)$, Eqs. (20), (23), and (24) can be used to calculate σ_l as function of ν. Results are plotted in Fig. 4 for several temperatures. For high temperatures $k_BT\gtrsim0.3\hbar\omega_c$, one gets the modified Drude result $\sigma_l=\sigma_H/(\omega_c\tau_{\rm gauss})$ with $\sigma_H=(e^2/h)\nu$ and $\hbar/\tau_{\rm gauss}=\sqrt{\pi/2}\Gamma$.

To proceed, we first investigate the effect of the Landau-level broadening Γ on the existence and width of the incompressible strips. Results of self-consistent calculations are shown in Fig. 5. The width of the incompressible strips shrinks with increasing temperature and with increasing level broadening. For $k_BT/\hbar\omega_c\lesssim0.04$ and $\Gamma/\hbar\omega_c\lesssim0.1$ clearly visible incompressible strips exist. Thus, collision broaden-

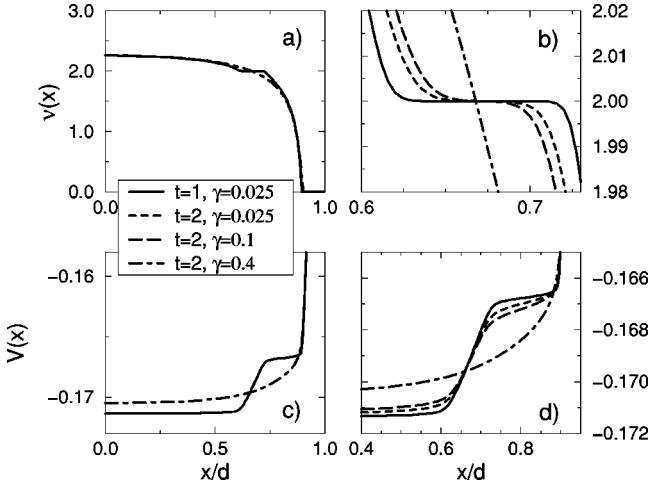

FIG. 5. Density profile [(a), (b)] and potential [(c), (d)] calculated with a Gaussian DOS; (b) and (d) show results in the region of the incompressible strip for several values of temperature, $k_BT/\hbar\omega_c = t/50$, and level broadening, $\gamma = \Gamma/\hbar\omega_c$. The solid and dash-dotted curves are plotted in (a) and (c) for one-half of the symmetric sample ($\alpha = 0.02$, $\hbar\omega_c/E_0 = 0.005$).

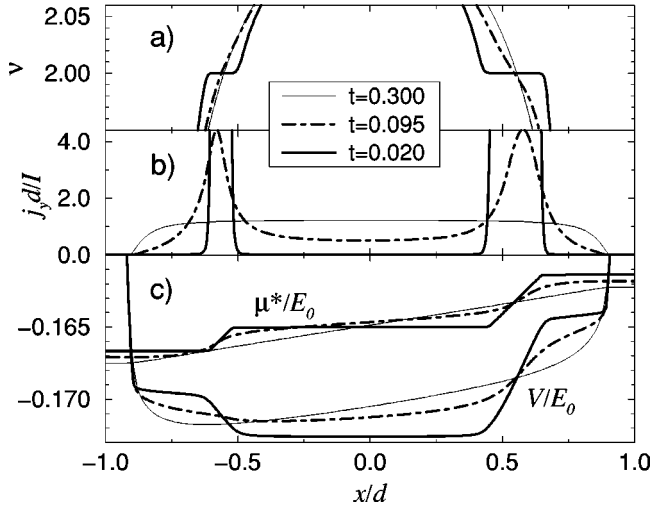

FIG. 6. Self-consistent results for (a) filling factor $\nu(x)$, (b) current density $j_y(x)$, and (c) electrostatic and electrochemical potentials, $V(x)$ and $\mu^\star(x)$, at three temperatures $t = k_BT/\hbar\omega_c$, calculated from the Gaussian model ($\alpha = 0.02$, $\hbar\omega_c/E_0 = 0.0053$, $\Gamma/\hbar\omega_c = 0.03$, $U_H = \hbar\omega_c$).

ing of the Landau DOS does not change the screening properties of the 2DEG qualitatively, provided the width of the Landau levels remains small enough as compared with the cyclotron energy.

Next we perform the self-consistent calculation of the charge and current densities and of the electrostatic and electrochemical potentials for the Gaussian model. To achieve convergence of the nested self-consistency loops for given values of temperature T, cyclotron energy $\Omega \equiv \hbar\omega_c$, and total current $I \propto U_H \equiv \Delta\mu^\star$, we proceed as follows. First we define the density profile by solving the linear integral equation [Eqs. (2) and (8)] for $T=0$, $B=0$, and $I=0$. Then we raise, still for $B=0$ and $I=0$, the temperature stepwise up to the value $k_BT = 0.3\Omega$ and solve at each step the nonlinear problem iteratively using a Newton-Raphson procedure. At this high temperature all quantum effects are smeared out, and we can replace the $B=0$ DOS by the Gaussian Landau DOS corresponding to the required Ω value without convergence problems. Now we raise stepwise the current until the required value is reached. This calculation is equivalent to the solution of the Drude problem discussed above. When self-consistency is achieved, we lower the temperature stepwise until the required (low) value is reached. In each step we iterate until full self-consistency is achieved, using the previous potential profile and the conductivity tensor with the density profile of the previous step as starting conditions.

Figure 6 shows the self-consistent results for several intermediate temperatures. At the highest temperature (thin solid lines) one observes Drude-like behavior: the current density [Fig. 6(b)] is proportional to the electron density [note that Fig. 6(a) shows the latter only near local filling factor $\nu(x)=2$, while $\nu(0)=2.25$] and the electrostatical and electrochemical potentials increase nearly linearly across the 2DEG. With decreasing temperature the 2DEG develops incompressible strips with low longitudinal resistivity and the current density is increasingly confined to the incompressible regions. Simultaneously the potentials develop a steplike behavior with variation across the incompressible strips and plateaus in the compressible regions.

To evaluate the current-induced electrostatic potential ΔV, we perform the self-consistent calculation with and without applied current and define $\Delta V(x) = V(x;I,B,T) - V(x;0,B,T)$. A typical result is shown in Fig. 7. The main difference between this result and Fig. 3 is that now the current density is confined more strictly to a narrow region along the incompressible strips (see dashed lines in the middle panels of the figures). The more rapid decrease of the current density from the large values in the incompressible strips to the small values in the compressible regions is caused mainly by the much steeper increase of $\sigma_l(\nu)$ with

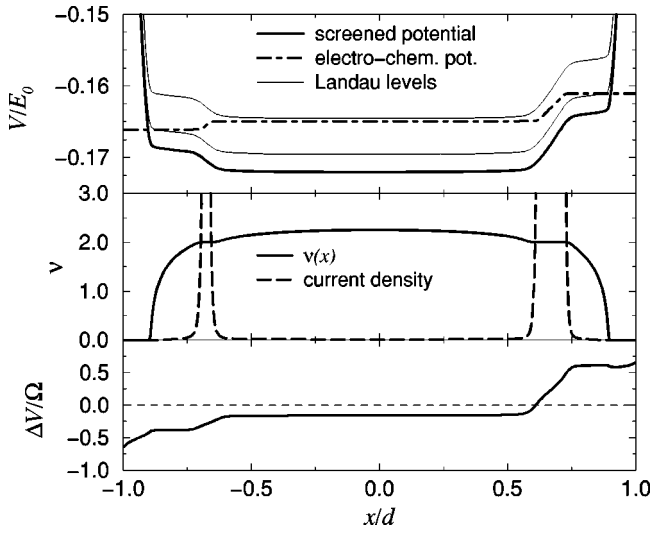

FIG. 7. Same Fig. 3, but with σ_l calculated from the Gaussian model (23) instead of Eq. (22), and only results for $U_H \equiv \Delta\mu^* = \Omega$ are shown ($\Gamma/\hbar\omega_c = 0.03$, all other parameters as in Fig. 3).

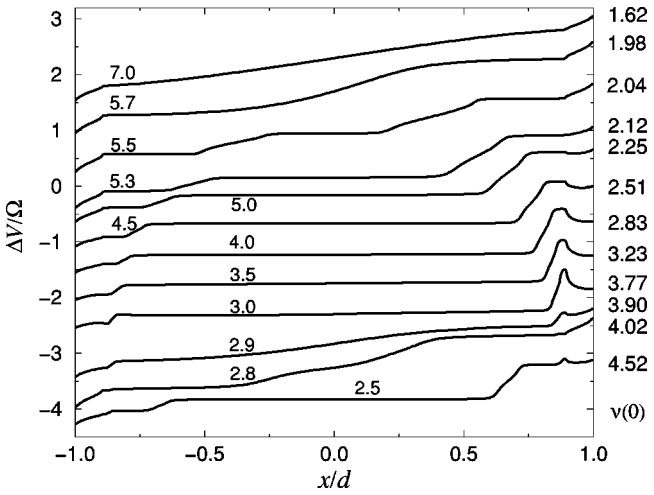

FIG. 8. Current-induced part $\Delta V(x)$ of the self-consistently calculated electrostatic potential in units of the cyclotron energy $\Omega = \hbar\omega_c$, for several values of Ω. The numbers in the figure indicate $(\Omega/E_0)\times 10^3$, those on the right-hand side the corresponding values of $\nu(0)$. For clarity, the traces are shifted vertically by an arbitrary amount.

increasing $|\nu-2|$ [see Fig. 4(b)]. The ratio between the values of the current density in the compressible region and those in the incompressible strips is also smaller, since we used near $\nu=2$ a smaller cutoff $\epsilon=\min[\sigma_l(\nu)/\sigma_H(\nu)]$ in the Gaussian model ($\epsilon=10^{-4}$) than in model (22) ($\epsilon=2\times10^{-3}$). As a consequence, the variation of the electrochemical potential (dash-dotted line of upper panel) and of the current-induced electrostatic potential (lower panel) is practically confined to the region of the incompressible strips.

The width and position of the incompressible strips and thus the locations of strong variation of the current-induced potential change strongly with varying magnetic field, i.e., with varying filling factors of the Landau levels. In Fig. 8 we show results for selected values of the magnetic field, leading to filling factors in the center of the Hall bar that vary between $\nu(0)=1.62$ and $\nu(0)=4.52$. The temperature is always chosen so low that the incompressible strips are well developed ($k_BT/\hbar\omega_c \lesssim 0.04$).

These results are easily understood. For $\hbar\omega_c \gtrsim 5.7\times10^{-3}E_0$ no incompressible strips exist, $\nu(x)<2$ for all $|x|<d$, and the current density is largest near the center of the sample, where the filling factor is largest and the longitudinal resistivity ($\rho_l \propto \sigma_l$) is smallest. Therefore the gradient of $\Delta V(x)$ is largest in the center of the Hall bar. If $\nu(0)<2$ is very close to 2, $\rho_l(x=0)$ is very small, the current density has a sharp maximum in the center, and the potential profile has a strongly nonlinear appearance (''type II'' behavior). If $\nu(0)$ becomes considerably smaller than 2, $\rho_l(x)$ has a broad maximum near $x=0$ and the current density profile follows essentially the density profile, similar to the Drude case. This leads to an essentially linear potential profile (''type I''), as is seen in the top curve of Fig. 8 for $\hbar\omega_c = 7.0\times10^{-3}E_0$, with $\nu(0)=1.62$.

For slightly lower magnetic field, an incompressible strip with $\nu(0)=2$ and (nearly) vanishing ρ_l occurs in the center. Then the variation of $\Delta V(x)$ is confined essentially to this strip (type II). With still decreasing $\hbar\omega_c$ this strip splits into two, which move with decreasing magnetic field towards to edges of the Hall bar. The electrochemical potential and (apart from some minor edge effects) the current-induced electrostatic potential then drop only across these incompressible strips (''type III''), as is seen in Fig. 8 for the curves with $2.04 \leqslant \nu(0) \leqslant 3.77$. As with further decreasing magnetic field the filling factor in the center region comes close to 4 and thus $\rho_l(x=0)$ becomes small, a considerable part of the current flows through this center region. Since at the same time the strips with local filling factor 2 become very narrow, for $\nu(0) \lesssim 4$ a considerable part of the induced potential drops in a broad center region (type II). For $\nu(0)>4$ the center region becomes again compressible, with constant $\Delta V(x)$, and the incompressible strips with $\nu(x)=4$, across which now most of the Hall voltage drops, move away from the center (type III). The lowest trace in Fig. 8 shows such a situation with tiny structures at the edges of the electron density profile which are due to the outer incompressible strips with local filling factor 2.

IV. CONCLUSIONS

Our results for the current-induced Hall-potential profile (Fig. 8) reproduce the characteristic features of the experiment of Ahlswede *et al.*[10] (Fig. 1), although in the experiment spin splitting is resolved whereas we assumed spin degeneracy. We therefore do not attempt a quantitative comparison. We also plot the electrostatic potential energy $V(x)=-e\phi(x)$ instead of $\phi(x)$, and we apparently consider the direction of the imposed current (or of the applied magnetic field) opposite to that considered in the experiment.

If the filling factors $\nu(0)$ in the center of the sample are close to, but below, integer values, the potential drops in a nonlinear fashion in a broad center region. For $\nu(0)$ values slightly larger than the integer values, the potential is constant in the center region and drops exclusively across the incompressible strips. Of course, our results show this characteristic behavior only near even integer values of $\nu(0)$, since we have neglected spin splitting, whereas in the experiment spin splitting is resolved and this behavior occurs also near small odd-integer values of $\nu(0)$.

This characteristic dependence of the Hall-potential profile on the magnetic field cannot be explained by the previous calculations assuming dissipationless Hall currents[17,18,25] and emphasizes the importance of dissipation. From the nice qualitative agreement of our results with the experimental data we conclude that our local equilibrium approach, which combines dissipative transport with screening effects and allows us to calculate electron and current density as well as electrostatic and electrochemical potentials self-consistently, contains most of the relevant physics. There is, however, room and need for improvements.

One desirable improvement concerns the effectiveness of narrow incompressible strips. To avoid numerical divergencies, we used a cutoff $\epsilon\cdot\sigma_H$ for σ_l at even integer values of ν, with $\epsilon=10^{-4}$. If we take the limit $\epsilon\to0$ and sufficiently low temperatures, $\rho_l(x)$ becomes exponentially small in the

incompressible strips. Then, according to Eq. (14), the electric field along the Hall bar and, therefore, the longitudinal resistance become exponentially small whenever an incompressible strip exists, and not only for a limited interval of magnetic field values in a plateau region of the QHE. To eliminate this unreasonable behavior, we should include a mechanism (other than the simple cutoff) that limits the current density in, and thereby the voltage drop across, narrow incompressible strips. Such a mechanism could make the incompressible strips with local filling factor $\nu(x)=2$ ineffective for magnetic fields with $\nu(0)\gtrsim 3$. This would turn the ''type III'' curves with $\nu(0)=3.23$ and 3.77 in Fig. 8 into quasilinear ''type I'' curves and would eliminate the tiny edge-near structures in the three lowest curves. Both changes would improve the agreement with the experiment.

Several physical effects may lead to such a mechanism. One is the nonlocal relation between the current density and the driving electric field, which we have approximated by a strictly local one. Another one is Joule heating, which is most effective where the current density is high and may destroy narrow incompressible strips, i.e., lead to a local breakdown of the QHE. A systematic treatment of heating effects will require the consideration of energy balance and heat conduction, as has recently been pointed out by Akera[29] in his hydrodynamic approach to quantum Hall systems in the breakdown regime. A consideration of the heating processes relevant under QHE conditions (e.g., ''quasielastic inter-Landau-level scattering'') (Refs. 30 and 31) may even demand a treatment beyond a local hydrodynamic approximation and require a more microscopic nonlocal description of stationary current-carrying nonequilibrium states intermediate between the zero-resistance quantum Hall state and the finite-resistance breakdown state.[32] Such a microscopic approach to heating and resistive processes may also open the possibility of a unified description of dissipative currents, which we have considered phenomenologically in the present paper, and nondissipative equilibrium currents, which we have mentioned in the Introduction but completely neglected in the calculations.

Finally we want to mention that in our model calculations the imposed current leads to a broadening of the incompressible strips on one side of the sample and to a narrowing of the corresponding strips on the opposite side (of course the strips exchange their role if we invert the direction of the current). This asymmetry is clearly seen in Fig. 8 and can also be observed in the experiment;[10] see Fig. 1. A systematic investigation of this effect may be of interest.

ACKNOWLEDGMENTS

We gratefully acknowledge helpful discussions with E. Ahlswede, G. Nachtwei, and J. Weis, and we thank E. Ahlswede and J. Weis for the permission to use Fig. 1. This work was supported by the Deutsche Forschungsgemeinschaft, SP ''Quanten-Hall-Systeme'' GE306/4.

[1] S. Komiyama and H. Hirai, Phys. Rev. B **54**, 2067 (1996).
[2] C. Wexler and D. J. Thouless, Phys. Rev. B **49**, 4815 (1994).
[3] M. R. Geller and G. Vignale, Phys. Rev. B **50**, 11 714 (1994).
[4] M. R. Geller and G. Vignale, Phys. Rev. B **52**, 14 137 (1995).
[5] N. Q. Balaban, U. Meirav, and H. Shtrikman, Phys. Rev. B **52**, R5503 (1995).
[6] E. Yahel, A. Palevski, and H. Shtrikman, Superlattices Microstruct. **22**, 537 (1997).
[7] G. Nachtwei, G. Lütjering, D. Weiss, Z. H. Liu, K. von Klitzing, and C. T. Foxon, Phys. Rev. B **55**, 6731 (1997).
[8] G. Nachtwei, Z. H. Liu, G. Lütjering, R. R. Gerhardts, D. Weiss, K. von Klitzing, and K. Eberl, Phys. Rev. B **57**, 9937 (1998).
[9] P. Weitz, E. Ahlswede, J. Weis, K. v. Klitzing, and K. Eberl, Physica E (Amsterdam) **6**, 247 (2000).
[10] E. Ahlswede, P. Weitz, J. Weis, K. v. Klitzing, and K. Eberl, Physica B **298**, 562 (2001).
[11] E. Ahlswede, J. Weis, K. v. Klitzing, and K. Eberl, Physica E (Amsterdam) **12**, 165 (2002).
[12] P. Weitz, E. Ahlswede, J. Weis, K. v. Klitzing, and K. Eberl, Appl. Surf. Sci. **157**, 349 (2000).
[13] D. B. Chklovskii, B. I. Shklovskii, and L. I. Glazman, Phys. Rev. B **46**, 4026 (1992).
[14] D. B. Chklovskii, K. A. Matveev, and B. I. Shklovskii, Phys. Rev. B **47**, 12 605 (1993).
[15] K. Lier and R. R. Gerhardts, Phys. Rev. B **50**, 7757 (1994).
[16] A. M. Chang, Solid State Commun. **74**, 871 (1990).
[17] D. Pfannkuche and J. Hajdu, Phys. Rev. B **46**, 7032 (1992).
[18] J. H. Oh and R. R. Gerhardts, Phys. Rev. B **56**, 13 519 (1997).
[19] R. Woltjer, R. Eppenga, J. Mooren, C. E. Timmering, and J. P. André, Europhys. Lett. **2**, 149 (1986).
[20] R. Woltjer, R. Eppenga, and M. F. H. Schuurmans, in *High Magnetic Fields in Semiconductor Physics*, Vol. 71 of *Springer Series in Solid-State Sciences*, edited by G. Landwehr (Springer-Verlag, Berlin, 1987), p. 104.
[21] R. R. Gerhardts and J. Groß , Phys. Rev. B **60**, 2561 (1999).
[22] K. Güven and R. R. Gerhardts (unpublished).
[23] L. I. Glazman and I. A. Larkin, Semicond. Sci. Technol. **6**, 32 (1991).
[24] U. J. Gossmann, A. Manolescu, and R. R. Gerhardts, Phys. Rev. B **57**, 1680 (1998).
[25] J. H. Oh and R. R. Gerhardts, Physica E (Amsterdam) **1**, 108 (1997).
[26] J. Groß and R. R. Gerhardts, Physica B **256-258**, 60 (1998).
[27] R. R. Gerhardts, Z. Phys. B **21**, 285 (1975).
[28] T. Ando, A. B. Fowler, and F. Stern, Rev. Mod. Phys. **54**, 437 (1982).
[29] H. Akera, J. Phys. Soc. Jpn. **70**, 1468 (2001).
[30] L. Eaves and F. W. Sheard, Semicond. Sci. Technol. **1**, 346 (1986).
[31] H. Akera, J. Phys. Soc. Jpn. **69**, 3174 (2000).
[32] K. Güven, R. R. Gerhardts, I. I. Kaya, B. E. Sagol, and G. Nachtwei, Phys. Rev. B **65**, 155 316 (2002).